IEEE Access
Multidisciplinary | Rapid Review | Open Access Journal

Received 8 April 2023, accepted 5 May 2023, date of publication 9 May 2023, date of current version 15 May 2023.

Digital Object Identifier 10.1109/ACCESS.2023.3274532

RESEARCH ARTICLE

An Improved Many-Objective Evolutionary Algorithm for Multi-Satellite Joint Large Regional Coverage

FENG LI[1,2,3], QIUHUA WAN[1,2], QIEN HE[3], XING ZHONG[3], KAI XU[3], AND RUIFEI ZHU[3]

[1]Changchun Institute of Optics, Fine Mechanics and Physics, Chinese Academy of Sciences, Changchun 130033, China
[2]Daheng college, University of Chinese Academy of Sciences, Beijing 100049, China
[3]Chang Guang Satellite Technology Company Ltd., Changchun 130102, China

Corresponding author: Qien He (heqien777@126.com)

This work was supported by the National Key Research and Development Program of China under Grant 2021YFC3101800.

ABSTRACT Multi-satellite joint regional coverage aims to select the optimal combination of satellite resources to acquire the image information of the specified area. Meanwhile, more than three objectives are usually considered simultaneously during this process. Therefore, it is a typical many-objective optimization problem that is NP-hard. Most existing many-objective optimization algorithms cannot preserve extreme solutions due to the failure of Pareto dominance. In this paper, through introducing the idea of S-CDAS into the traditional NSGA-III, an improved many-objective evolutionary algorithm named NSGA-III for extreme solutions preservation (ESP-NSGA-III) is proposed with problem-specific genetic operations to generate regional coverage schemes. A comparative study is conducted with other six state-of-the-art many-objective evolutionary algorithms. Hypervolume (HV) and pure diversity (PD) metrics are used to evaluate the performance of algorithms. The simulation results show that ESP-NSGA-III has good comprehensive performance and improves the diversity of original algorithms. The maximum difference of the coverage rate between ESP-NSGA-III and other six algorithms is 0.2576 so that satisfactory regional coverage scheme can be obtained by ESP-NSGA-III. Our proposed methods are not only applicable to regional coverage tasks, but also have important reference significance for solving other real-world problems.

INDEX TERMS Many-objective optimization, multi-satellite joint, NSGA-III, regional coverage, S-CDAS.

I. INTRODUCTION

Earth observation satellites (EOSes) dynamically monitor and analyze the natural environment, economic crops, traffic conditions, and sudden disasters, etc. by acquiring images of specified areas on the Earth's surface [1]. However, it is hard to achieve full coverage of large region by single satellite due to the size of the field of view (FOV). With the continuous increase of the number of satellites on orbit, multi-satellite joint mode provides us with opportunities for rapid large regional coverage. The regional coverage process aims to select the optimal combination of satellites from all available satellite resources so that they can acquire the area images to the utmost extent in a cooperative manner while satisfying various constraints. Consequently, the problem of multi-satellite joint regional coverage is a typical combinatorial optimization problem, which has been proven to be NP-hard [2]. To solve this large-scale planning problem within reasonable computational time, heuristic and meta-heuristic algorithms such as tabu search [3], greedy search [4], ant colony optimization [5], [6], genetic algorithm [7], [8] and so on are more suitable than the exact methods.

Due to the realistic demand, meanwhile, regional coverage tasks always have to optimize multiple objectives simultaneously, such as total profit, image quality, timeliness, cost and so on. Therefore, multi-objective evolutionary algorithms (MOEAs) have been widely explored by researchers in recent years. Aiming at multi-satellite planning for

The associate editor coordinating the review of this manuscript and approving it for publication was Massimo Cafaro.

large-region image acquisition, Chen et al. [9] established an optimization model with two objectives of maximum target region coverage and minimum satellite resource utilization, and employed non-dominated sorting genetic algorithm (NSGA-II) [10] for model solving. With the goal of maximizing the total profit, minimizing the number of strips, and minimizing the overlap of strips, Xu et al. [11] transformed the regional coverage problem into a set covering problem (SCP), established a mathematical model, and then used the NSGA-II algorithm to generate the optimal planning scheme. In the context of disaster emergency response, Niu et al. [12] established a multi-satellite joint coverage model with the objectives of maximum coverage rate, minimum imaging completion time, minimum average spatial resolution, and minimum average slewing angle. Then NSGA-II was employed to obtain the optimal solution of satellite planning. Li et al. [13] established a mathematical model with minimum the number of strips, minimum the overlap ratio of strips, maximum coverage rate, and minimum task completion time as four objectives, and selected the Two-Archive2 algorithm [14] to formulate a regional coverage planning scheme.

Although the above studies have achieved certain results, few objectives are considered and the algorithms used are relatively simple. Usually, multi-objective optimization problems (MOPs) with more than three objectives are referred to as many-objective optimization problems (MaOPs) [15]. The performance of traditional MOEAs, such as NSGA-II, deteriorates seriously when handling MaOPs. The main reason is that the selection pressure based on Pareto dominance degrades severely with the number of objectives increasing. A large number of algorithms have been proposed for MaOPs. NSGA-III [16], the improved version of NSGA-II, is one of the most representative algorithms. In NSGA-III, reference-points based method is adopted to replace crowding distance, which reduces the impact of Pareto dominance by increasing diversity. However, since the Pareto dominance is not changed, the phenomenon of dominance resistance will still appear with the continuous iteration of the algorithm. As a result, all candidate solutions will be distributed on the same Pareto front (PF) at an iteration, which makes them incomparable. This condition has serious negative effects when dealing with practical problems. Taking regional coverage tasks as an example, coverage rate is the most important objective in most instances, and clients hope to optimize other objectives under the premise of maximizing coverage rate. However, the failure of Pareto dominance makes candidate solutions can only be selected by the niche-preservation operation, resulting in a certain probability that the solution with the maximum coverage rate (extreme solution for short) cannot be selected for the next iteration. This will not only reduce the efficiency of genetic operations, but more importantly, the algorithm cannot provide a satisfactory planning scheme for clients.

To solve this issue, researchers have made a lot of efforts on modifying the Pareto dominance to increase the degree of distinction between two candidate solutions. Yuan et al. [17] designed θ-dominance to replace the Pareto dominance and proposed θ-NSGA-III, which can ensure both convergence and diversity. Tian et al. [18] proposed a new dominance relation, named strengthened dominance relation (SDR), to balance convergence and diversity by developing a niching technique based on the angles between the candidate solutions. On this basis, Gu et al. [19] modified the measure of convergence of candidate solutions in SDR and proposed DDR. He et al. [20] adopted the concept of fuzzy logic to define a fuzzy Pareto domination relation, which can continuously differentiate solutions into different degrees of optimality beyond the classification of the original Pareto dominance. Sato et al. [21] controlled the degree of expansion or contraction of the dominance area of solutions (CDAS) using a user-defined parameter S inducing a ranking of solutions that is different to conventional Pareto dominance. Because CDAS relies heavily on the parameter S, they further modified CDAS and proposed S-CDAS [22] to self-control dominance area for each solution. However, the starting point of most researches is to improve the convergence or diversity of the algorithm on test problems such as DTLZ [23] and WFG [24]. More importantly, these algorithms are not suitable for dealing with practical problems as they cannot guarantee to preserve extreme solutions. Few algorithms, such as S-CDAS, can preserve extreme solutions, but its diversity are relatively poor [18]. Therefore, the purpose of this paper is to propose a novel MOEA, which can preserve extreme solutions and improve the diversity of the original algorithm, to solve many-objective regional coverage problem.

The remainder of this paper is organized as follows. Section II introduces the problem description and data resources, including objectives, satellite information, and the process of regional decomposition. Then the NSGA-III and S-CDAS frameworks are briefly reviewed in Section III. The details of the proposed algorithm and coding strategies are given in Section IV. Finally, in Section V, experimental simulations are conducted to validate the proposed algorithm. The simulation results demonstrate that the ESP-NSGA-III has better performance than the other algorithms.

II. PROBLEM DESCRIPTION AND DATA RESOURCES

A. PROBLEM DESCRIPTION

For the convenience of readers, the variable symbols and explanations are first summarized in Table 1.

1) PROBLEM SETTING

According to the satellite conditions and practical applications, the following assumptions are adopted.

- The satellite lens can only swing left and right but not forward and backward.
- Once an observation task is started, it cannot be interrupted or cancelled until it is finished.
- At most one strip can be selected per transit per satellite, i.e.,

$$\sum_{k=1}^{|N_{ij}|} x_{ijk} \leq 1, \forall i \in [1, |S|], \forall j \in [1, |O_i|] \quad (1)$$

- The length of all strips is limited between the minimum imaging length and maximum imaging length of the corresponding satellite.
- The data transmission planning is not within the scope of this study.
- Satellite storage capacity and electricity are infinite.

TABLE 1. Variable symbols and explanation.

Variable symbols	Explanation
$s_i \in S$	The i-th satellite
S	The set of satellites
$o_{ij} \in O_i$	The j-th transit of the i-th satellite
O_i	The set of transits of the i-th satellite
N_{ij}	The set of strips in which the i-th satellite decomposes the target region in the j-th transit
x_{ijk}	0-1 variable, indicating whether the k-th strip of the i-th satellite in the j-th transit is selected
$area_{ijk}$	The area covered by x_{ijk}
$overlap$ ()	The function to calculate the overlap area of strips
r_i	The resolution of the i-th satellite
sa_{ijk}	The swing angle of k-th strip of the i-th satellite in the j-th transit
SA_i	The maximum swing angle of i-th satellite
$area_T$	The area of the target region to be covered
n_s	The number of strips in the final regional coverage planning

2) OBJECTIVES

In this paper, five objectives are to be optimized simultaneously. The first objective is maximizing the coverage rate (equivalent to maximizing the profit), which is the most important one in our research. The second objective is minimizing the overlap ratio of selected strips and the third objective is minimizing the number of selected strips. These two objectives are to increase the utilization efficiency of the satellites and reduce cost. The overlap ratio is defined as the ratio of the strips' overlap area within the target region to the total coverage area. The fourth objective is minimizing the average resolution and the fifth objective is minimizing the average swing angle. These two objectives are to improve the image quality. For unification, the first objective is transformed to a minimization problem. Five objectives are formulated as follows:

- Maximize the coverage rate:

$$\min 1 - \frac{(\bigcup_{i=1}^{|S|} \bigcup_{j=1}^{|O_i|} \bigcup_{k=1}^{|N_{ij}|} x_{ijk} area_{ijk}) \cap area_T}{area_T} \tag{2}$$

- Minimize the overlap ratio of selected strips:

$$\min \frac{(\sum_{i=1}^{|S|} \sum_{j=1}^{|O_i|} \sum_{k=1}^{|N_{ij}|} overlap(x_{ijk})) \cap area_T}{(\bigcup_{i=1}^{|S|} \bigcup_{j=1}^{|O_i|} \bigcup_{k=1}^{|N_{ij}|} x_{ijk} area_{ijk}) \cap area_T} \tag{3}$$

- Minimize the number of selected strips:

$$\min n_s = \min \sum_{i=1}^{|S|} \sum_{j=1}^{|O_i|} \sum_{k=1}^{|N_{ij}|} x_{ijk} \tag{4}$$

- Minimize the average resolution:

$$\min \frac{\sum_{i=1}^{|S|} \sum_{j=1}^{|O_i|} \sum_{k=1}^{|N_{ij}|} x_{ijk} r_i}{n_s} \tag{5}$$

- Minimize the average swing angle:

$$\min \frac{\sum_{i=1}^{|S|} \sum_{j=1}^{|O_i|} \sum_{k=1}^{|N_{ij}|} x_{ijk} sa_{ijk} / SA_i}{n_s} \tag{6}$$

B. DATA RESOURCES

Three kinds of satellites (GF03B, KF01, and GF02) used for simulation experiments are independently developed by *Chang Guang satellite technology CO., LTD* and are in service. Some parameters of the satellites are listed in Table 2.

Sichuan province, China is chosen as the target region to be covered. Its area is about 485,000 km^2, which is too big to be observed by a single satellite, providing an opportunity for multi-satellite joint coverage.

C. REGIONAL DECOMPOSITION

Considering the target region is far much larger than single observation scope of any satellite, it is a common measure to decompose the target into discrete strips. Fig.1 shows the process of regional decomposition and strip selection. The red line in Fig.1b is the ground track of one satellite, and the green rectangular frame is the biggest observable range of the satellite determined by its swath and maximum swing angle. Since the swing angle is a continuous variable, one satellite can actually create countless corresponding strips. To make the problem computable, as shown in Fig.1c, the range of swing angles are divided into a group of discrete values with a step $\Delta\lambda = 0.5$km. This approach can obtain a finite number of strips within each observing opportunity. Finally, only one strip will be selected randomly from the strips set to participate in the regional coverage task, as shown in Fig.1d. As a result, a total of 20,344 strips were obtained from all satellites and used as input of the proposed algorithm.

III. REVIEW OF METHODS

In this section, several basic definitions in MaOPs are first given. Then the original NSGA-III and S-CDAS, which are the basis of our proposed algorithm, are briefly introduced.

A. MANY-OBJECTIVE OPTIMIZATION CONCEPTS AND DEFINITIONS

A minimized many-objective optimization problem including M ($M > 3$) objective functions is defined as follows:

$$\begin{cases} \text{Minimize } \boldsymbol{F}(\boldsymbol{x}) = (f_1(\boldsymbol{x}), f_2(\boldsymbol{x}), \cdots, f_i(\boldsymbol{x}), \cdots, f_M(\boldsymbol{x})) \\ \text{Subjectto } \boldsymbol{x} \in D \end{cases} \tag{7}$$

where $\boldsymbol{x}$ is a feasible candidate solution in the solution space D, and $f_i(\boldsymbol{x})$ ($i = 1, 2, \cdots, M$) is the i-th objective function to be minimized. Generally, the Pareto dominance principle is widely used in MOPs and MaOPs for distinguishing

TABLE 2. Some parameters of the satellites.

Satellite IDs	The number of transits	Swath (km)	Resolution (m)	Maximum swing angle (°)[a]	Maximum imaging length (km)[a]	Minimum imaging length (km)[a]
GF03B01	3	17	1.00	15	615	70
GF03B02	4	17	1.00	15	615	70
GF03B03	6	17	1.00	15	615	70
GF03B04	6	17	1.00	15	615	70
GF03B05	4	17	1.00	15	615	70
GF03B06	3	17	1.00	15	615	70
KF01A	5	135	0.75	3	1400	70
KF01B	5	150	0.50	3	1400	70
GF02A	5	40	0.75	15	1190	70
GF02B	4	40	0.75	15	1190	70

[a]These values are selected for simulation and are slightly different from the true condition.

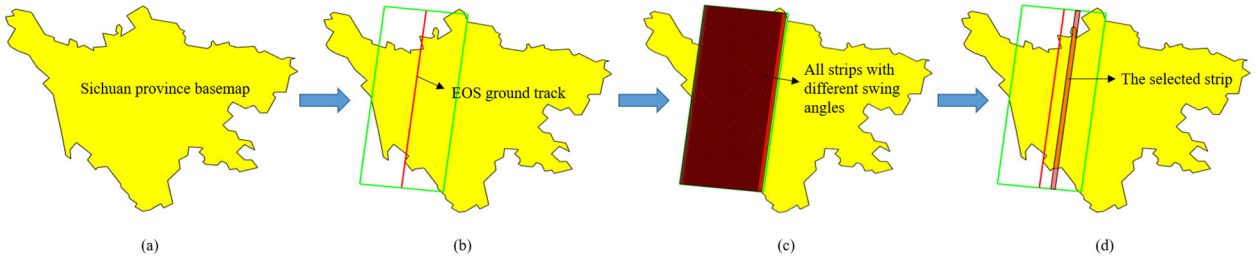

FIGURE 1. The process of regional decomposition and strip selection.

the quality of two candidate solutions $\boldsymbol{x}$ and $\boldsymbol{y}$. Specifically, if inequalities:

$$\begin{cases} \forall i \in \{1, 2, \cdots, M\} : f_i(\boldsymbol{x}) \leq f_i(\boldsymbol{y}) \wedge \\ \exists j \in \{1, 2, \cdots, M\} : f_j(\boldsymbol{x}) < f_j(\boldsymbol{y}) \end{cases} \tag{8}$$

are satisfied, candidate solution $\boldsymbol{x}$ is said to Pareto dominate $\boldsymbol{y}$, denoted as $f(\boldsymbol{x}) \preceq f(\boldsymbol{y})$ [25]. If $\boldsymbol{x}$ cannot be Pareto dominated by all other solutions in D, $\boldsymbol{x}$ is said to be Pareto optimal. Hence, the set of Pareto solutions (POS) is defined as:

$$POS = \{\boldsymbol{x} \in D | \neg \exists \boldsymbol{y} \in D : f(\boldsymbol{x}) \preceq f(\boldsymbol{y})\} \tag{9}$$

and the PF is defined as:

$$PF = f(\boldsymbol{x}) | \boldsymbol{x} \in POS \tag{10}$$

B. NSGA-III

The basic framework of NSGA-III remains similar to that of NSGA-II. The most notable improvements of NSGA-III are the introduction of reference points and the environment selection mechanism related to reference points. Firstly, Das and Dennis's systematic approach [26] is usually employed to construct structured reference points on a normalized hyperplane. Specifically, if p divisions are considered along each objective, the total number of reference points (H) in an M-objective problem is given by:

$$H = \left(\frac{M + p - 1}{p} \right) \tag{11}$$

The following steps are iterated until the termination criterion is satisfied. At the t-th generation of NSGA-III, several genetic operations such as selection, crossover, and mutation are carried out on the current population P_t (of size N) to generate the offspring population Q_t. Then $R_t = P_t \cup Q_t$ is obtained where the size of R_t is $2N$. To select best N individuals from R_t to create P_{t+1} for next generation, the nondominated sorting based on Pareto dominance is used, which divides R_t into different levels (F_1, F_2, and so on). Starting from F_1, all individuals belonging to this level are put into a new population S_t one at a time until the size of S_t is equal to or larger than N for the first time. Supposing the last level included is the l-th level, then individuals in $S_t F_l$ are already selected for composing P_{t+1} and individuals from the level $l+1$ onward are removed. Individuals in F_l are fed into the environment selection operation to select the remaining $N - |S_t F_l|$ individuals to maintain diversity of solutions.

The environment selection operation consists of several parts:

(1) The objective values of the individuals are normalized using the ideal and extreme points so that they have an identical range.

(2) The perpendicular distance between an individual in S_t and a reference line (joining the origin with a reference point) is computed. Each individual in S_t is then associated with a reference point having the minimum perpendicular distance.

(3) Performing the niche-preservation operation. It is the actual step of selecting individuals in environment selection operation, which works as follows:

- The niche count ρ_j for the j-th reference point, defined as the number of individuals in $S_t F_l$ that are associated with the j-th reference point, is computed.
- Reference point set $J_{min} = \{j: argmin_j \rho_j$ having the minimum ρ_j value is identified. If $|J_{min}| > 1$, one

reference point $\bar{j} \in J_{min}$ is chosen randomly. If the level F_l does not have any individual associated with the $\bar{j}$-th reference point, the reference point is not considered for the current generation, meanwhile, J_{min} is recomputed and $\bar{j}$ is reselected. Otherwise, the value of $\rho_{\bar{j}}$ is further considered. If $\rho_{\bar{j}} \geq 1$, an individual in F_l that is associated with the $\bar{j}$-th reference point is randomly selected into population P_{t+1}, and the value of $\rho_{\bar{j}}$ is incremented by one. If $\rho_{\bar{j}} = 0$, the individual having the minimum perpendicular distance to the $\bar{j}$-th reference line is selected into population P_{t+1} and the value of $\rho_{\bar{j}}$ is also incremented by one.

- Niche-preservation operation is repeated until the size of P_{t+1} reaches N. More details about NSGA-III can be found in the literature [16].

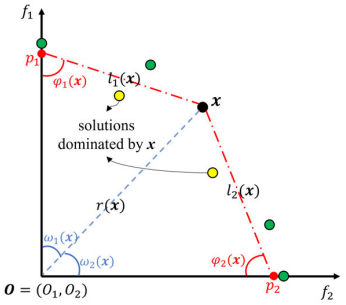

FIGURE 2. The schematic diagram of reclassification of solutions in F_1 by S-CDAS. Seven individuals (solid circles) are non-dominated each other in original Pareto dominance, but after S-CDAS, yellow individuals become dominated by x.

C. S-CDAS

S-CDAS modifies the dominance area of each individual by referring to extreme solutions in the population, thereby enhancing the probability of two individuals being comparable on MaOPs. In this way, the algorithm can guarantee the extreme solutions always in the top front. For a bi-objective maximization problem, Fig.2 shows the schematic diagram of the reclassification of several solutions in F_1.

Specifically, S-CDAS reclassifies the solutions in each front $F_j(j = 1, 2, \cdots)$ derived from the original Pareto dominance according to the following steps.

Step 1: Move the origin to $\boldsymbol{O} = (O_1, O_2, \cdots, O_M)$ in objective space. $O_i = f_i^{min}(i = 1, 2, \cdots, M)$, where f_i^{min} is the minimum value of the i-th objective function in F_j.

Step 2: Create a set of landmark vectors $L = \{p_1, p_2, \cdots, p_M$, where $p_i = (O_1, O_2, \cdots, f_i^{max} - \delta, \cdots, O_M)$. f_i^{max} is the maximum value of the i-th objective function and δ is a tiny constant value.

Step 3: Repeat the following steps for all solutions in F_j:

Step 3.1: For a solution $\boldsymbol{x}$, calculate $\varphi(\boldsymbol{x}) = (\varphi_1(\boldsymbol{x}), \varphi_2(\boldsymbol{x}), \cdots, \varphi_M(\boldsymbol{x}))$ by (12). $\varphi_i(\boldsymbol{x})$ is the angle determined by $\boldsymbol{x}$ and the landmark vector $\boldsymbol{p}_i$ in the i-th objective function.

$$\varphi_i(\boldsymbol{x}) = \sin^{-1}\left(\frac{r(\boldsymbol{x}) \cdot \sin(\omega_i(\boldsymbol{x}))}{l_i(\boldsymbol{x})}\right) \tag{12}$$

where $r(\boldsymbol{x})$ is the norm of $\boldsymbol{F}(\boldsymbol{x})$, $\omega_i(\boldsymbol{x})$ is the declination angle between $\boldsymbol{F}(\boldsymbol{x})$ and $f_i(\boldsymbol{x})$, and $l_i(\boldsymbol{x})$ is Euclidean distance between $\boldsymbol{x}$ and the landmark vector $\boldsymbol{p}_i$.

Step 3.2: Modify objective values of all other solutions $\boldsymbol{y} \in F_j$ by the following equation:

$$f_i'(\boldsymbol{y}) = \frac{r(\boldsymbol{y}) \cdot \sin(\omega_i(\boldsymbol{y}) + \varphi_i(\boldsymbol{x}))}{\sin(\varphi_i(\boldsymbol{x}))} \tag{13}$$

Step 4: Compare the modified $\boldsymbol{F}'(\boldsymbol{x})$ and all other $\boldsymbol{F}'(\boldsymbol{y})$. If $\boldsymbol{F}'(\boldsymbol{x}) \prec \boldsymbol{F}'(\boldsymbol{y})$, the solution $\boldsymbol{y}$ is said to be dominated by $\boldsymbol{x}$, and the rank of $\boldsymbol{y}$ is incremented by one. Smaller rank corresponds to higher front, and larger rank corresponds to lower front. When the loop ends, new dominance relations are obtained for all individuals in the current population. More details about S-CDAS can refer to literature [22].

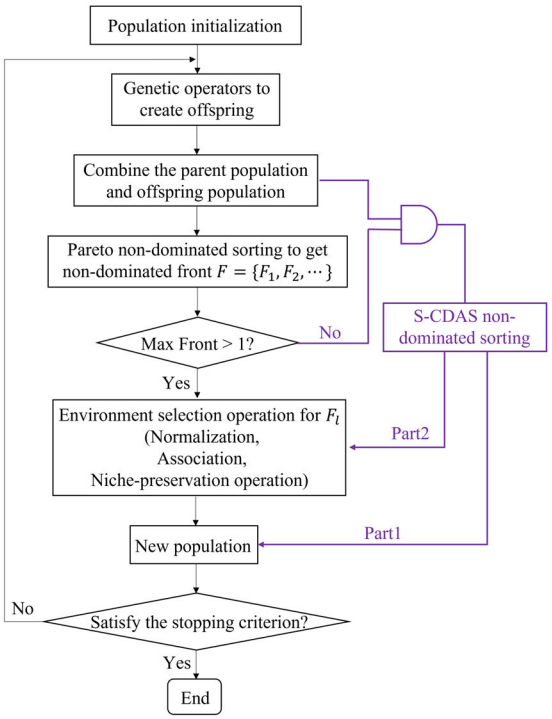

FIGURE 3. The flowchart of proposed ESP-NSGA-III.

IV. FRAMEWORK OF THE PROPOSED ALGORITHM

A. THE PROPOSED ESP-NSGA-III

The principle of the algorithm is to ensure that extreme solutions can be preserved in each iteration, and the diversity of algorithm can be improved simultaneously. The flowchart of ESP-NSGA-III consisting of two parts is shown in Fig.3. Specifically, at the beginning of the iteration, original Pareto non-dominated sorting is used to divide solutions into different fronts. If the maximum front is greater than 1, it means that extreme solutions must belong to the first front, which guarantees that extreme solutions will be preserved and involved to the next population. Therefore, the black part of Fig.3 is the same with the original NSGA-III.

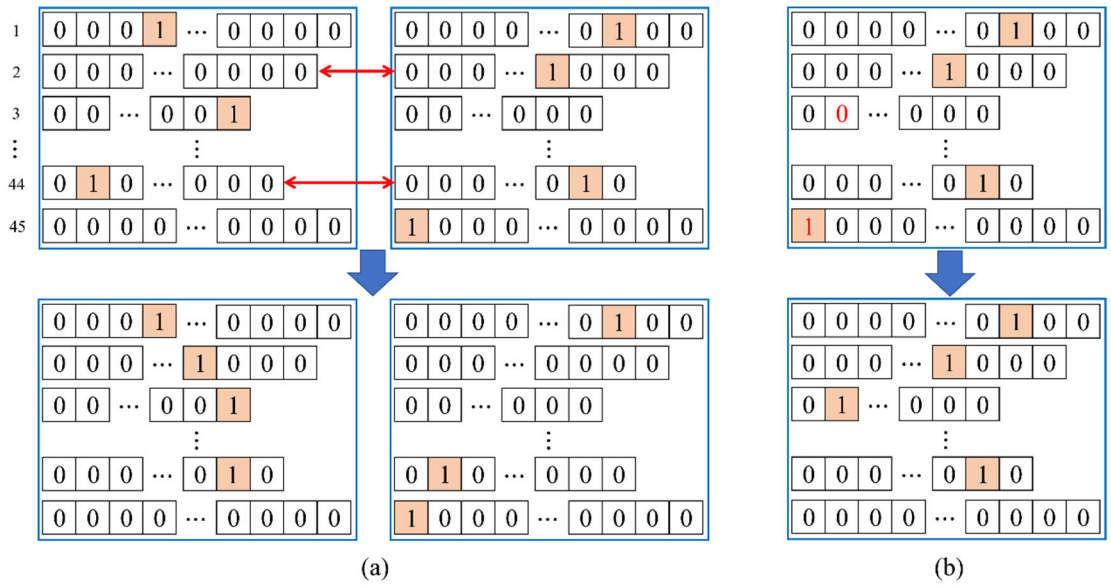

FIGURE 4. The schematic diagram of encoding, crossover, and mutation operators. One blue frame is one individual in population, and each row vector presents a satellite. (a) crossover operator. (b) mutation operator.

As the iteration continues and selection pressure decreases, however, the maximum front is equal to 1 in a certain iteration. In this case, Pareto dominance will no longer be effective, and S-CDAS dominance is directly performed on the combined population R_t instead. Please note that the strategy used here is a bit different from the original S-CDAS that reclassifies the solutions in each existing front. After S-CDAS non-dominated sorting, all individuals are divided into two parts according to their front levels. The part1 are n individuals with lower front that directly enter the new population. The part2 are the remaining individuals that are fed into environment selection operation to select the rest of the new population. The purpose of this way is to take advantage of the environment selection operation in NSGA-III to increase the diversity of the algorithm. The determination of hyperparameter n will be discussed in Section V.

B. PROBLEM CODING

Due to the specificity of the problem, binary encoding, which is different from the original NSGA-III, is employed. The schematic diagram is shown in Fig.4. Specifically, one satellite with k strips is represented as a vector of length k. Each element in the vector is either 1 or 0; 1 means that the corresponding strip is selected, and 0 means that the strip is not selected, so an all-0 vector means that the satellite is not involved in the regional coverage task. Please note that different satellites have different numbers of strips, so one individual is a matrix consisting of vectors of different lengths.

C. SELECTION

Niching based selection proposed in U-NSGA-III [27] is used in our framework for two reasons. One is to ensure the structural integrity of genetic algorithms, and the other is that some studies have shown that the method can improve the convergence of the algorithm to a certain degree [28], [29]. The details of the method can be found in [27].

D. CROSSOVER

Random multi-point crossover is used in the crossover operator, which is shown as Fig.4a. Specifically, if the random number is less than the crossover probability, n (n is randomly generated and less than 15) rows of two individuals are randomly selected and exchanged each other.

E. MUTATION

Single-point mutation operator is employed and shown as Fig.4b. For an individual, if the random number is less than the mutation probability, five rows are randomly selected firstly for mutation. For each row, if there exists an allele value of 1, let the 1 be 0; otherwise, if all elements are 0, a locus is randomly selected and a value of 1 is assigned to this locus.

F. PERFORMANCE EVALUATION METRICS

Most real-world problems do not know the true PF distribution in advance, resulting in some metrics usually used for classic test problems will no longer work well. In this paper, therefore, HV [30] and PD [31] are selected to evaluate the algorithm performance in practical problem. On one hand, the HV value is used to evaluate the algorithm comprehensively. The HV value of a given solution set is defined as the area covered by it with respect to a set of predefined reference points $\boldsymbol{Z}$ in the objective space. A larger HV value indicates the better convergence as well as diversity of the points in PF. On the other hand, PD is further used to illustrate that the proposed algorithm can make up for the lack of diversity in

TABLE 3. HV values of 7 algorithms over 40 runs.

Run	NSGA-III	S-CDAS	Fuzzy-NSGA-II	Fuzzy-NSGA-III	SDR-NSGA-II	SDR-NSGA-III	ESP-NSGA-III
1	0.5158	0.5056	0.3954	0.3356	0.5233	0.5861	0.5159 (3)
2	0.4956	0.5126	0.4011	0.3495	0.5246	0.5920	0.5264 (2)
3	0.5165	0.4998	0.3938	0.3415	0.5189	0.5884	0.5206 (2)
4	0.5203	0.5034	0.4109	0.3369	0.5267	0.5928	0.5198 (4)
5	0.4933	0.4961	0.4087	0.3478	0.5240	0.5866	0.5187 (3)
6	0.4979	0.5087	0.3956	0.3345	0.5169	0.5917	0.5245 (2)
7	0.5063	0.5101	0.3859	0.3298	0.5203	0.5859	0.5166 (3)
8	0.5140	0.4953	0.3905	0.3489	0.5245	0.5905	0.5211 (3)
9	0.5278	0.4972	0.3862	0.3455	0.5278	0.5842	0.5236 (4)
10	0.5205	0.5002	0.3989	0.3320	0.5180	0.5908	0.5158 (4)
11	0.5295	0.4988	0.3860	0.3521	0.5159	0.6074	0.5140 (4)
12	0.5375	0.5030	0.3986	0.3625	0.5392	0.5970	0.5011 (5)
13	0.5064	0.4938	0.4192	0.3463	0.5405	0.5963	0.5508 (2)
14	0.5236	0.5199	0.4271	0.3498	0.5244	0.5846	0.5360 (2)
15	0.5119	0.5199	0.4214	0.3473	0.5187	0.6110	0.5513 (2)
16	0.5317	0.5117	0.3840	0.3612	0.5270	0.6036	0.5090 (5)
17	0.5284	0.5035	0.3962	0.3587	0.5415	0.6092	0.5507 (2)
18	0.4984	0.5233	0.3913	0.3316	0.5419	0.6030	0.5437 (2)
19	0.5331	0.5121	0.3953	0.3320	0.5363	0.6144	0.5318 (4)
20	0.5395	0.5283	0.4273	0.3345	0.5457	0.6143	0.5242 (5)
21	0.5157	0.5257	0.4063	0.3543	0.5452	0.5888	0.5142 (5)
22	0.5342	0.5043	0.4160	0.3328	0.5186	0.6019	0.5414 (2)
23	0.5194	0.5119	0.4204	0.3633	0.5357	0.6055	0.5126 (4)
24	0.4977	0.5039	0.3880	0.3527	0.5304	0.5974	0.5035 (4)
25	0.5000	0.5149	0.4233	0.3318	0.5171	0.6097	0.5422 (2)
26	0.5103	0.5219	0.3850	0.3585	0.5437	0.5867	0.5369 (3)
27	0.5274	0.5198	0.4158	0.3605	0.5309	0.5843	0.5393 (2)
28	0.5313	0.4950	0.4150	0.3625	0.5397	0.5801	0.5353 (3)
29	0.5295	0.5229	0.4144	0.3473	0.5169	0.5854	0.5230 (3)
30	0.5055	0.5183	0.3983	0.3594	0.5356	0.5923	0.5400 (2)
31	0.5337	0.5105	0.4167	0.3491	0.5280	0.5921	0.5178 (4)
32	0.5349	0.5194	0.3887	0.3615	0.5256	0.5865	0.5263 (3)
33	0.5344	0.5064	0.4202	0.3523	0.5219	0.5824	0.5399 (2)
34	0.4968	0.5091	0.3852	0.3629	0.5394	0.6080	0.5072 (4)
35	0.5331	0.4963	0.4055	0.3290	0.5444	0.5981	0.5250 (4)
36	0.5139	0.5122	0.4121	0.3454	0.5319	0.5913	0.5223 (3)
37	0.4933	0.5237	0.4076	0.3294	0.5163	0.5999	0.5412 (2)
38	0.5040	0.5087	0.4041	0.3468	0.5143	0.6038	0.5302 (2)
39	0.5303	0.5068	0.3978	0.3526	0.5303	0.5900	0.5443 (2)
40	0.4986	0.5010	0.3941	0.3380	0.5379	0.6021	0.5138 (3)
Average	0.5173	0.5094	0.4032	0.3467	0.5290	0.5954	0.5268 (3)
+/≈/− (*p*-value)	− (4.4740e-03)	− (5.3644e-09)	− (5.8788e-38)	− (2.0487e-40)	≈ (0.4091)	+ (6.9646e-27)	

the original methods. The larger the PD value is, the better the diversity of the algorithm is. In addition, the paired-sample *t*-test is adopted at a significant level of 0.05 to check if the comparison results are statistically significant, especially when the performance metric values of two approximative fronts are very close to each other.

V. EXPERIMENTAL RESULTS AND DISCUSSION

A. PARAMETER SETTINGS

The parameters are set as follows. The size of population is 210. The maximum number of iterations is 500. The crossover probability is 0.8 and mutation probability is 0.1. To examine the performance of the proposed approach, six state-of-the-art algorithms with the same genetic operations are used for results comparison. They are NSGA-III, S-CDAS, Fuzzy-NSGA-II, Fuzzy-NSGA-III, SDR-NSGA-II, and SDR-NSGA-III. PlatEMO [32] is employed to implement the NSGA-III and SDR-NSGA-II. All algorithms are executed 40 independent runs with different initial populations to verify generalization and different algorithms use the same initial population in each run for convenience of comparison.

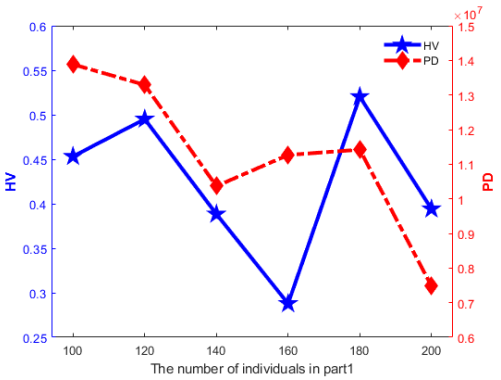

FIGURE 5. The trend of HV and PD values with the increase of hyperparameter *n*.

B. THE PERFORMANCE OF ESP-NSGA-III

1) THE DETERMINATION OF HYPERPARAMETER N

The hyperparameter *n* presents the number of individuals in part1 and needs to be determined in advance to guarantee the performance of the algorithm. Therefore, the ESP-NSGA-III was executed with six values of *n* from 100 to 200, and the

TABLE 4. PD values of 7 algorithms over 40 runs.

Run	NSGA-III	S-CDAS	Fuzzy-NSGA-II	Fuzzy-NSGA-III	SDR-NSGA-II	SDR-NSGA-III	ESP-NSGA-III
1	6.7022e+06	3.0888e+06	3.1807e+06	1.5714e+06	4.8495e+06	5.0980e+06	1.2986e+07 (1)
2	7.4378e+06	3.1435e+06	2.8367e+06	1.7990e+06	4.9455e+06	5.1363e+06	9.5894e+06 (1)
3	7.4132e+06	2.6762e+06	3.2838e+06	2.0758e+06	4.9796e+06	4.9429e+06	1.0938e+07 (1)
4	6.9885e+06	3.1480e+06	3.2764e+06	1.7042e+06	4.7736e+06	4.7045e+06	9.6954e+06 (1)
5	6.7450e+06	2.9794e+06	3.0170e+06	1.8512e+06	4.5693e+06	4.7988e+06	1.2859e+07 (1)
6	7.1641e+06	2.6585e+06	3.1902e+06	1.6343e+06	4.5746e+06	5.2437e+06	9.3172e+06 (1)
7	6.8864e+06	2.7671e+06	2.8280e+06	1.9508e+06	4.6288e+06	4.7490e+06	1.2167e+07 (1)
8	7.1596e+06	2.9281e+06	2.7820e+06	1.6531e+06	4.9204e+06	5.1868e+06	1.2324e+07 (1)
9	7.4280e+06	3.1745e+06	3.0537e+06	1.8036e+06	4.6271e+06	4.9999e+06	1.2514e+07 (1)
10	6.7776e+06	3.1418e+06	2.7586e+06	1.6377e+06	4.9415e+06	5.1951e+06	1.1811e+07 (1)
11	6.9558e+06	2.9285e+06	3.0479e+06	1.9216e+06	4.6742e+06	5.2258e+06	1.0553e+07 (1)
12	6.8307e+06	3.0095e+06	2.9232e+06	1.8310e+06	4.7893e+06	4.9233e+06	1.2033e+07 (1)
13	7.2392e+06	2.7587e+06	2.8376e+06	1.8415e+06	4.7850e+06	4.8987e+06	1.0670e+07 (1)
14	6.8986e+06	3.0099e+06	2.8339e+06	1.8988e+06	4.8054e+06	4.9522e+06	1.2515e+07 (1)
15	6.9682e+06	3.1695e+06	2.8253e+06	1.7638e+06	4.6999e+06	4.9011e+06	1.1376e+07 (1)
16	6.9557e+06	2.7981e+06	3.1404e+06	1.7605e+06	4.7360e+06	5.1287e+06	1.0549e+07 (1)
17	7.1283e+06	3.0795e+06	3.0057e+06	1.8821e+06	4.7365e+06	4.9299e+06	1.2377e+07 (1)
18	7.1248e+06	3.1867e+06	2.8123e+06	1.8887e+06	4.9928e+06	4.8124e+06	1.2285e+07 (1)
19	7.2729e+06	3.0240e+06	2.8490e+06	1.6667e+06	4.5760e+06	5.0586e+06	1.2137e+07 (1)
20	7.3218e+06	3.0738e+06	3.1920e+06	1.6090e+06	4.7284e+06	4.9278e+06	1.0296e+07 (1)
21	7.2725e+06	2.8862e+06	3.0327e+06	1.6199e+06	4.9061e+06	4.9315e+06	1.0385e+07 (1)
22	7.3817e+06	2.9566e+06	3.0516e+06	1.6500e+06	4.8174e+06	4.7842e+06	1.1918e+07 (1)
23	6.9083e+06	2.7716e+06	2.8643e+06	1.6600e+06	4.6893e+06	5.1836e+06	1.1674e+07 (1)
24	7.3584e+06	2.9234e+06	3.1815e+06	1.8190e+06	4.9558e+06	4.9789e+06	1.1027e+07 (1)
25	6.8271e+06	2.9128e+06	3.0396e+06	1.6103e+06	4.5919e+06	4.7888e+06	1.2500e+07 (1)
26	6.9444e+06	2.8794e+06	3.0641e+06	1.7653e+06	4.6936e+06	5.2025e+06	1.0976e+07 (1)
27	6.8053e+06	3.1175e+06	2.9821e+06	1.8375e+06	4.9491e+06	4.8908e+06	1.2584e+07 (1)
28	7.2030e+06	2.9527e+06	3.1466e+06	1.6402e+06	4.8458e+06	5.0569e+06	1.1021e+07 (1)
29	7.3429e+06	3.1130e+06	2.7902e+06	1.6826e+06	4.8580e+06	5.0809e+06	1.1061e+07 (1)
30	7.1434e+06	3.1056e+06	3.0772e+06	1.7012e+06	4.7633e+06	4.8500e+06	1.1883e+07 (1)
31	6.8933e+06	2.8773e+06	3.2241e+06	1.6605e+06	4.6136e+06	5.2300e+06	1.0703e+07 (1)
32	7.1014e+06	2.7807e+06	2.9968e+06	1.7133e+06	4.9779e+06	5.0826e+06	1.0905e+07 (1)
33	7.1406e+06	2.7747e+06	3.1089e+06	1.8804e+06	4.9472e+06	5.0206e+06	9.9112e+06 (1)
34	6.9130e+06	3.0369e+06	2.9169e+06	1.7049e+06	4.7468e+06	5.1845e+06	1.1851e+07 (1)
35	6.9945e+06	2.9409e+06	3.0841e+06	1.8715e+06	4.9257e+06	5.0285e+06	1.1252e+07 (1)
36	7.2296e+06	3.1575e+06	2.9034e+06	1.7935e+06	4.6963e+06	4.7607e+06	1.1511e+07 (1)
37	7.1318e+06	2.9378e+06	3.1898e+06	1.7941e+06	4.7154e+06	4.9913e+06	1.1974e+07 (1)
38	6.8854e+06	2.8193e+06	3.1879e+06	1.8557e+06	4.9077e+06	5.1540e+06	1.0183e+07 (1)
39	7.0282e+06	2.9930e+06	3.1762e+06	1.8708e+06	4.5947e+06	5.1180e+06	1.2159e+07 (1)
40	6.9091e+06	3.1428e+06	3.1355e+06	1.8486e+06	4.7109e+06	5.0881e+06	1.2327e+07 (1)
Average	7.0703e+06	2.9706e+06	3.0207e+06	1.7681e+06	4.7810e+06	5.0055e+06	1.1420e+07 (1)
+/≈/− (p-value)	− (3.2737e-26)	− (1.8212e-39)	− (6.8960e-38)	− (6.9838e-41)	− (4.6720e-34)	− (3.3251e-33)	

HV and PD values corresponding to different n are recorded in Fig.5. On one hand, as the number of individuals in part1 increases, the HV values do not show obvious law of change and are concentrated between 0.25 and 0.55. The minimum value is 0.2878 when $n = 160$ and the maximum value is 0.5203 when $n = 180$. On the other hand, we can see that as n increases, PD values approximately present a downward trend. When n is between 100 and 180, PD values fluctuate slightly, but it decreases significantly when $n = 200$. This phenomenon is consistent with our expectation, and the reason may be that only 10 individuals are selected through environment selection operation, which causes a decline in algorithm diversity. By considering the HV and PD values comprehensively, $n = 180$ is finally chosen for all experiments to balance convergence and diversity.

Some existing MOEAs such as fuzzy-based methods and CDAS are heavily parameters dependent, which seriously affects the execution efficiency of algorithms. For example, the parameter S in CDAS has to be found out experimentally and when $S < 0.5$, there is a tendency to deteriorate diversity of obtained solutions [22]. Compared with the original methods, n is the only new parameter added to ESP-NSGA-III. Fig.5 shows that the value of n can be chosen in a big range without seriously affecting the performance of the algorithm. In other words, the algorithm is insensitive to the parameter n.

2) CONVERGENCE AND DIVERSITY ANALYSIS

The HV and PD values of seven algorithms over 40 independent runs are presented in Table 3 and Table 4, respectively. The numbers in brackets are ranks of ESP-NSGA-III among seven algorithms for each run. We further test the null hypothesis that there exists no significant difference between HV and PD values from ESP-NSGA-III to other six algorithms. The p-value, obtained by paired-sample t-test, is the probability that the null hypothesis is true. In other words, if the p-value is less than 0.05, we have the reason to reject the null hypothesis and believe that the existing difference is significant. "+", "−", and "≈" indicate that the average of 40 runs is significantly better, significantly worse and similar to that obtained by ESP-NSGA-III, respectively.

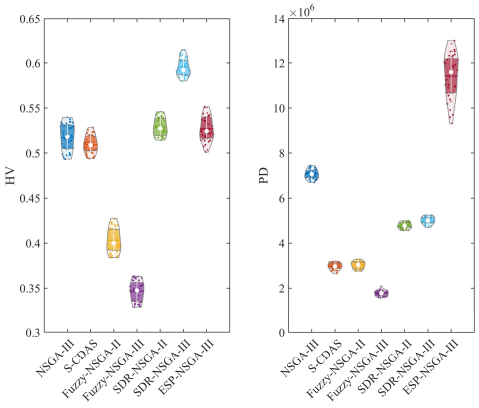

FIGURE 6. The violin plot to present the HV and PD values of 7 algorithms on 40 independent runs.

From Table 3 it can be seen that over 40 runs, fuzzy-based methods always get the worst HV values, and SDR-NSGA-III always gets the best. In most runs (36/40), the proposed algorithm can always rank in the top half of seven algorithms and the biggest difference between it and SDR-NSGA-III is just 0.1 (the 34th run). From the average, the performance of ESP-NSGA-III ranks the third and is significantly better than that of NSGA-III and S-CDAS, which are the basic frameworks of ESP-NSAG-III. It is worth noting that although the average of SDR-NSGA-II is slightly better than that of our algorithm, the statistical test result (p-value=0.4091) shows that there is no noticeable difference among the HV values of these two algorithms. This means that SDR-NSGA-II cannot be guaranteed to get better solutions than ESP-NSGA-III in the statistical sense.

In terms of diversity in Table 4, it can be seen that ESP-NSGA-III significantly outperforms all other algorithms and is the only one whose PD value exceeds 1e+07. S-CDAS has the second lowest average PD values, illustrating that S-CDAS cannot maintain the diversity of algorithms with the increase of objective dimension, which is consistent with the previous studies [18], [19]. NSGA-III gets good PD values due to the niche-preservation operation. However, ESP-NSGA-III has an obvious improvement in diversity when compared to NSGA-III, which can attribute to the introduction of extreme solutions. The results show that in the high-dimensional objective space, the diversity maintenance of NSGA-III is obviously lacking [19].

A violin plot is also provided in Fig.6 for more intuitive comparisons. The dark parts indicate the interval between the first quartile (Q1) and the third quartile (Q3). From Fig.6 we can see that although the PD values of ESP-NSGA-III are more scattered, the smallest value is still much larger than that of other algorithms. In summary, ESP-NSGA-III is an effective algorithm for solving MaOPs, which can improve the diversity of original algorithms while ensuring good convergence.

C. APPLICATION IN MANY-OBJECTIVE REGIONAL COVERAGE TASK

In this section, ESP-NSGA-III was applied to many-objective regional coverage task to check its ability to deal with practical problems.

1) THE EFFECT OF EXTREME SOLUTION PRESERVATION COMPARED WITH SIX STATE-OF-THE-ART MOEAS

The ability to preserve extreme solutions is the biggest improvement of ESP-NSGA-III compared with most other MOEAs. For multi-satellite joint large regional coverage problem, the algorithm is expected to always preserve the individual with the maximum coverage rate in each generation. Fig.7 shows the comparison results of the maximum coverage rate change trend during the 500 iterations of algorithms. Blue line presents the maximum coverage rate obtained by ESP-NSGA-III. It can be seen that the curve always maintains an upward trend, which proves that the algorithm can indeed preserve the extreme solutions. In addition, the maximum coverage rate still increases after 447 iterations, demonstrating that the genetic operations designed in our algorithm work well and rarely let the algorithm fall into local optimum. On the contrary, from the curve obtained by NSGA-III (orange line in Fig.7a) it can be found that when the number of iterations is small (first 40 iterations in this paper), the curve presents an upward trend, because the Pareto dominance has not expired at this time. As the algorithm continues to iterate, however, all candidate solutions are distributed on the same PF, leading to the disappearance of extreme solutions in the population. Therefore, the curve fluctuates up and down and the maximum coverage rate is only 0.9117 after 500 iterations, which is much smaller than 0.9980 obtained by ESP-NSGA-III. The same phenomenon also occurs in fuzzy-based and SDR-based algorithms, as shown in Fig.7(b)-(e). Although these algorithms have been proven to achieve good convergence and diversity on test problems, they are not suitable for practical problems as they cannot obtain user-satisfactory solutions. S-CDAS is another one that can preserve extreme solutions, as shown in Fig.7(f). However, the convergence of the algorithm is much worse than ESP-NSGA-III and the maximum coverage rate at 500th iteration is only 0.9547. Besides, the poor diversity of S-CDAS cannot provide enough evolutionary space for solutions, which also results in poor performance in maximum coverage rate.

2) REGIONAL COVERAGE SCHEME COMPARED WITH SIX STATE-OF-THE-ART MOEAS

In order to demonstrate that the proposed algorithm can generate a more reasonable regional coverage scheme, the result is compared with the above six state-of-the-art MOEAs. After 500 iterations, each algorithm generates 210 solutions. For the sake of fairness, the solution with the largest coverage rate at the 500th iteration of each algorithm is chosen for

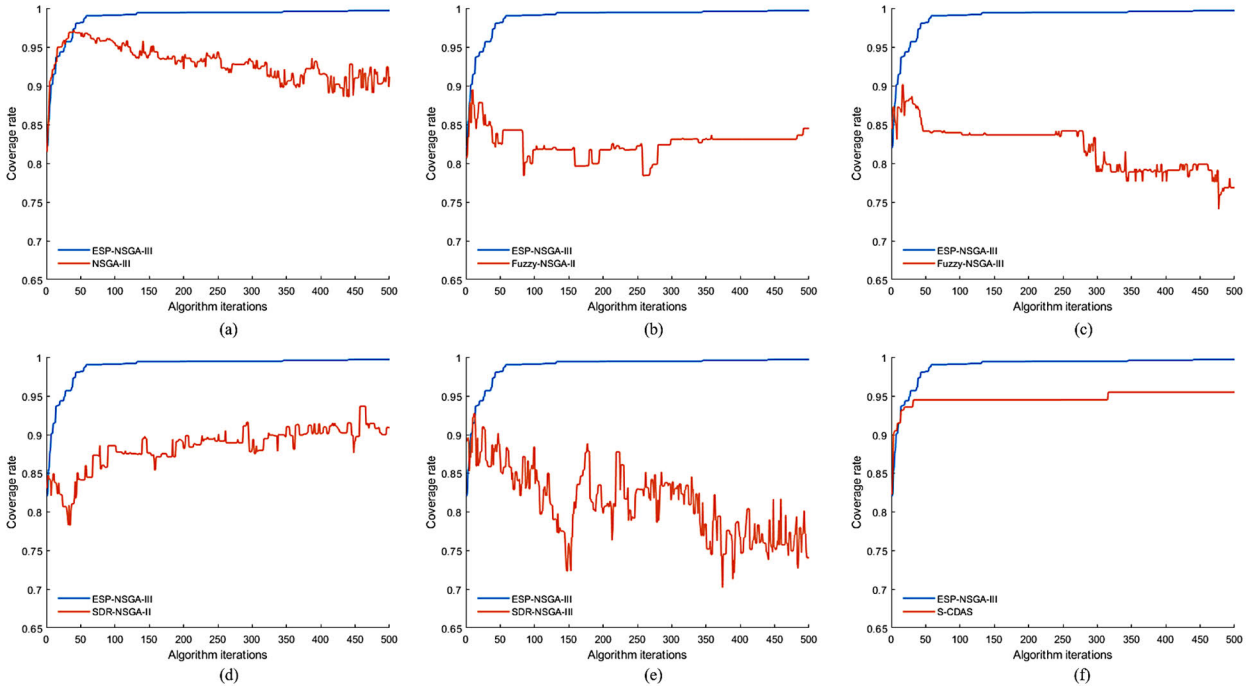

FIGURE 7. Comparison results of the maximum coverage rate change trend.

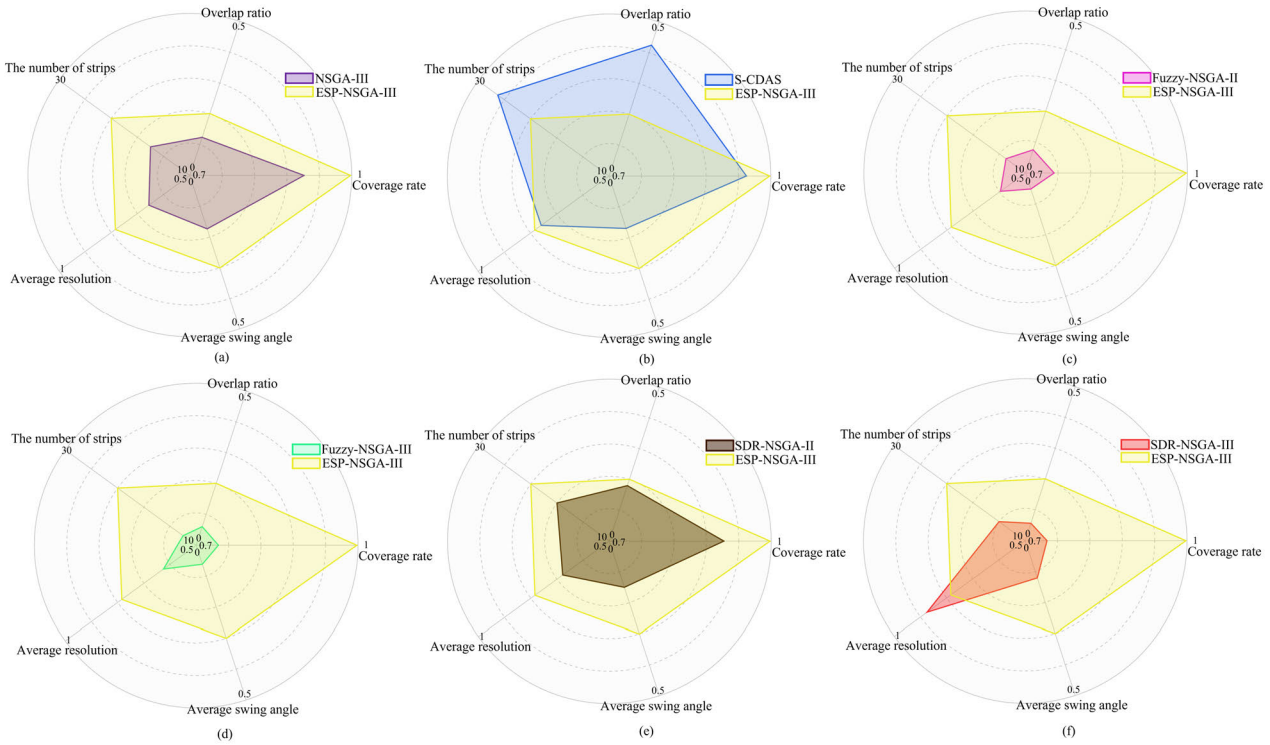

FIGURE 8. Radar charts of the values of 5 objectives obtained by 7 MOEAs.

comparison. The values of five objectives obtained by different algorithms are shown in Fig.8 and are summarized in Table 5. In radar charts, the coordinate intervals are [1, 0.7] for coverage rate, [0, 0.5] for overlap ratio, [10], [29] for the

TABLE 5. Comparison results of 5 objectives obtained by ESP-NSGA-III and other comparison algorithms.

	ESP-NSGA-III	NSGA-III	S-CDAS	Fuzzy-NSGA-II	Fuzzy-NSGA-III	SDR-NSGA-II	SDR-NSGA-III
Coverage rate	0.9980	0.9117	0.9547	0.7528	0.7686	0.9123	0.7404
Overlap ratio[a]	0.2008	0.1236	0.4245	0.0753	0.0602	0.1813	0.0567
The number of strips	22	16	27	13	12	18	14
Average resolution[a]	0.7841	0.6563	0.7593	0.5962	0.6250	0.6780	0.8750
Average swing angle[a]	0.3004	0.1735	0.1702	0.0520	0.0616	0.1506	0.1207

[a]The values of these three objectives are normalized using the equation (3), (5), and (6) defined in "2) OBJECTIVES" respectively.

number of strips, [1, 0.5] for average resolution, and [0, 0.5] for average swing angle. The coverage rate is expected to be as high as possible and the other four objectives are expected to be as small as possible. Taking four algorithms (NSGA-III, Fuzzy-NSGA-II, Fuzzy-NSGA-III, and SDR-NSGA-II) as examples, from Fig.8 it can be found that their areas are completely inside the area of ESP-NSGA-III, which means four objectives except for coverage rate of these algorithms are better than those of ESP-NSGA-III. This can also be found in Table 5. The phenomenon is easy to explain. These algorithms have been shown to be unable to preserve extreme solutions during the training (Fig.7), so the coverage rate of the final regional coverage scheme may be relatively low, followed by smaller overlap ratio and the number of strips. However, in practical applications, such schemes cannot meet the demands of clients as they cannot acquire the most images of the target area.

In summary, all simulation results show that the proposed algorithm can not only obtain a regional coverage scheme with satisfactory coverage rate by introducing the extreme solution preservation mechanism, but also optimize the rationality of the scheme from other objective dimensions. This demonstrates the excellent performance of the algorithm in solving practical MaOPs. What's more, like other MOEAs, ESP-NSGA-III can provide different solutions to meet the different task demands using a single run. For instance, when a client wants the highest quality image while allowing a slight sacrifice in coverage rate, we can directly choose a corresponding scheme from the 210 solutions instead of re-running the algorithm after changing the objective.

VI. CONCLUSION

In this paper, an improved MOEA named ESP-NSGA-III is proposed to address many-objective regional coverage problem. Problem-specific genetic operations are designed, and traditional Pareto dominance are modified to preserve extreme solutions. Six state-of-the-art MOEAs are used to prove the effectiveness of the proposed algorithm. Comparison results show that ESP-NSGA-III has the best diversity with regard to PD and good comprehensive performance with regard to HV. Real-world simulation results demonstrate that the algorithm can preserve the extreme solutions so that satisfactory regional coverage schemes can be generated. The maximum difference of the coverage rate between ESP-NSGA-III and other six algorithms is 0.2576. Most importantly, ESP-NSGA-III is not only applicable to regional coverage tasks, but also have important reference significance for solving other real-world problems.

In future studies, we will compare the ESP-NSGA-III with other types of MOEAs on more benchmark problems and practical applications. Real encoding genetic operations with simulated binary crossover (SBX) and polynomial mutation can also be explored to compare the performance with binary encoding. In addition, there is still room for improvement in the HV value of the proposed algorithm.

REFERENCES

[1] G. Denis, A. Claverie, X. Pasco, J.-P. Darnis, B. de Maupeou, M. Lafaye, and E. Morel, "Towards disruptions in Earth observation? New Earth Observation systems and markets evolution: Possible scenarios and impacts," *Acta Astronautica*, vol. 137, pp. 415–433, Aug. 2017.

[2] W.-C. Lin, D.-Y. Liao, C.-Y. Liu, and Y.-Y. Lee, "Daily imaging scheduling of an Earth observation satellite," *IEEE Trans. Syst., Man, Cybern. A, Syst. Humans*, vol. 35, no. 2, pp. 213–223, Mar. 2005.

[3] D. Habet, M. Vasquez, and Y. Vimont, "Bounding the optimum for the problem of scheduling the photographs of an Agile Earth Observing Satellite," *Comput. Optim. Appl.*, vol. 47, no. 2, pp. 307–333, Oct. 2010.

[4] F. Perea, R. Vazquez, and J. Galan-Viogue, "Swath-acquisition planning in multiple-satellite missions: An exact and heuristic approach," *IEEE Trans. Aerosp. Electron. Syst.*, vol. 51, no. 3, pp. 1717–1725, Jul. 2015.

[5] Z. Zhang, N. Zhang, and Z. Feng, "Multi-satellite control resource scheduling based on ant colony optimization," *Exp. Syst. Appl.*, vol. 41, no. 6, pp. 2816–2823, 2014.

[6] G. Wu, J. Liu, M. Ma, and D. Qiu, "A two-phase scheduling method with the consideration of task clustering for Earth observing satellites," *Comput. Oper. Res.*, vol. 40, no. 7, pp. 1884–1894, Jul. 2013.

[7] M. A. A. Mansour and M. M. Dessouky, "A genetic algorithm approach for solving the daily photograph selection problem of the SPOT5 satellite," *Comput. Ind. Eng.*, vol. 58, no. 3, pp. 509–520, Apr. 2010.

[8] S.-W. Baek, S.-M. Han, K.-R. Cho, D.-W. Lee, J.-S. Yang, P. M. Bainum, and H.-D. Kim, "Development of a scheduling algorithm and GUI for autonomous satellite missions," *Acta Astronautica*, vol. 68, nos. 7–8, pp. 1396–1402, Apr./May 2011.

[9] Y. Chen, M. Xu, X. Shen, G. Zhang, Z. Lu, and J. Xu, "A multi-objective modeling method of multi-satellite imaging task planning for large regional mapping," *Remote Sens.*, vol. 12, no. 3, p. 344, Jan. 2020.

[10] K. Deb, A. Pratap, S. Agarwal, and T. Meyarivan, "A fast and elitist multiobjective genetic algorithm: NSGA-II," *IEEE Trans. Evol. Comput.*, vol. 6, no. 2, pp. 182–197, Apr. 2002.

[11] Y. Xu, X. Liu, R. He, Y. Chen, and Y. Chen, "Multi-objective satellite scheduling approach for very large areal observation," in *Proc. IOP Conf Ser., Mater. Sci. Eng.*, 2018, Art. no. 012037.

[12] X. Niu, H. Tang, and L. Wu, "Satellite scheduling of large areal tasks for rapid response to natural disaster using a multi-objective genetic algorithm," *Int. J. Disaster Risk Reduction*, vol. 28, pp. 813–825, Jun. 2018.

[13] X. M. Li, "Two-Archive2 algorithm for large-scale polygon targets observation scheduling problem," in *Proc. Int. Conf. Inf. Technol. Manag. Eng.*, 2017, pp. 23–24.

[14] B. Li, J. Li, K. Tang, and X. Yao, "An improved two archive algorithm for many-objective optimization," in *Proc. IEEE Congr. Evol. Comput. (CEC)*, Jul. 2014, pp. 2869–2876.
[15] A. García-Nájera and A. López-Jaimes, "An investigation into many-objective optimization on combinatorial problems: Analyzing the pickup and delivery problem," *Swarm Evol. Comput.*, vol. 38, pp. 218–230, Feb. 2018.
[16] K. Deb and H. Jain, "An evolutionary many-objective optimization algorithm using reference-point-based nondominated sorting approach, Part I: Solving problems with box constraints," *IEEE Trans. Evol. Comput.*, vol. 18, no. 4, pp. 577–601, Aug. 2014.
[17] Y. Yuan, H. Xu, B. Wang, and X. Yao, "A new dominance relation-based evolutionary algorithm for many-objective optimization," *IEEE Trans. Evol. Comput.*, vol. 20, no. 1, pp. 16–37, Feb. 2016.
[18] Y. Tian, R. Cheng, X. Zhang, Y. Su, and Y. Jin, "A strengthened dominance relation considering convergence and diversity for evolutionary many-objective optimization," *IEEE Trans. Evol. Comput.*, vol. 23, no. 2, pp. 331–345, Apr. 2019.
[19] Q. Gu, Q. Xu, and X. Li, "An improved NSGA-III algorithm based on distance dominance relation for many-objective optimization," *Exp. Syst. Appl.*, vol. 207, Nov. 2022, Art. no. 117738.
[20] Z. He, G. G. Yen, and J. Zhang, "Fuzzy-based Pareto optimality for many-objective evolutionary algorithms," *IEEE Trans. Evol. Comput.*, vol. 18, no. 2, pp. 269–285, Apr. 2014.
[21] H. Sato, H. E. Aguirre, and K. Tanaka, "Controlling dominance area of solutions and its impact on the performance of MOEAs," in *Proc. Int. Conf. (EMO)*, 2007, pp. 5–20.
[22] H. Sato, H. E. Aguirre, and K. Tanaka, "Self-controlling dominance area of solutions in evolutionary many-objective optimization," in *Proc. Asia–Pacific Conf. Simulated Evol. Learn.*, 2010, pp. 455–465.
[23] K. Deb, L. Thiele, M. Laumanns, and E. Zitzler, "Scalable test problems for evolutionary multiobjective optimization," in *Evolutionary Multiobjective Optimization*. London, U.K.: Springer, 2005, pp. 105–145.
[24] S. Huband, P. Hingston, L. Barone, and L. While, "A review of multiobjective test problems and a scalable test problem toolkit," *IEEE Trans. Evol. Comput.*, vol. 10, no. 5, pp. 477–506, Oct. 2006.
[25] T. Glasmachers, "A fast incremental BSP tree archive for non-dominated points," in *Proc. Int. Conf. Evol. Multi-Criterion Optim.*, 2017, pp. 252–266.
[26] I. Das and J. E. Dennis, "Normal-boundary intersection: A new method for generating the Pareto surface in nonlinear multicriteria optimization problems," *SIAM J. Optim.*, vol. 8, no. 3, pp. 631–657, Jul. 1998.
[27] H. Seada and K. Deb, "U-NSGA-III: A unified evolutionary optimization procedure for single, multiple, and many objectives: Proof-of-principle results," in *Proc. Int. Conf. Evol. Multi-Criterion Optim.*, 2015, pp. 34–49.
[28] H. Seada and K. Deb, "Effect of selection operator on NSGA-III in single, multi, and many-objective optimization," in *Proc. IEEE Congr. Evol. Comput. (CEC)*, May 2015, pp. 2915–2922.
[29] Q. Liu, X. Liu, J. Wu, and Y. Li, "An improved NSGA-III algorithm using genetic K-means clustering algorithm," *IEEE Access*, vol. 7, pp. 185239–185249, 2019.
[30] E. Zitzler and L. Thiele, "Multiobjective evolutionary algorithms: A comparative case study and the strength Pareto approach," *IEEE Trans. Evol. Comput.*, vol. 3, no. 4, pp. 257–271, Nov. 1999.
[31] H. Wang, Y. Jin, and X. Yao, "Diversity assessment in many-objective optimization," *IEEE Trans. Cybern.*, vol. 47, no. 6, pp. 1510–1522, Jun. 2017.
[32] Y. Tian, R. Cheng, X. Zhang, and Y. Jin, "PlatEMO: A MATLAB platform for evolutionary multi-objective optimization [educational forum]," *IEEE Comput. Intell. Mag.*, vol. 12, no. 4, pp. 73–87, Nov. 2017.

FENG LI received the B.Eng. and M.Eng. degrees from Harbin Engineering University, Harbin, China, in 2011 and 2013, respectively. He is currently a Research and Development Engineer and the Head of the Department with Chang Guang Satellite Technology Company Ltd. His research interests include optical remote sensing satellite control system design and mission planning optimization.

QIUHUA WAN received the Ph.D. degree in optical engineering from the University of Chinese Academy of Sciences, Beijing, China, in 2009. She is currently a Researcher with the Research and Development Center for Precision Instruments and Equipment, Changchun Institute of Optics, Fine Mechanics and Physics. Her research interests include electro-optical displacement precision measurement and planning optimization.

QIEN HE received the B.Eng. and M.Eng. degrees from Tianjin University, Tianjin, China, in 2019 and 2022, respectively. He is currently a Research and Development Engineer with Chang Guang Satellite Technology Company Ltd. His research interests include multi-objective evolutionary algorithms and constellation scheduling and planning.

XING ZHONG received the Ph.D. degree in optical engineering from the Changchun Institute of Optics, Fine Mechanics and Physics, Chinese Academy of Sciences (CAS). From 2009 to 2014, he was an Associate Professor with the Changchun Institute of Optics, Fine Mechanics and Physics, CAS. He was entitled as a Full Professor with the Changchun Institute of Optics, Fine Mechanics and Physics, CAS, in 2015, and took part in the work founding Chang Guang Satellite Technology Company Ltd. (CGSTL). He is currently the Chief Engineer with CGSTL. He is also a Professor with the University of CAS.

KAI XU received the Ph.D. degree in optical engineering from the Changchun Institute of Optics, Fine Mechanics and Physics, Chinese Academy of Sciences. He is currently the Deputy General Manager with Chang Guang Satellite Technology Company Ltd. His research interests include satellite attitude control mathematical and physical simulation systems.

RUIFEI ZHU received the B.E. degree from Jilin University, Changchun, China, in 2009, and the Ph.D. degree from the Changchun Institute of Optics, Fine Mechanics and Physics, Chinese Academy of Sciences, Changchun, in 2014. He is currently with Chang Guang Satellite Technology Company Ltd. His research interests include remote sensing image processing and mining.